HHS Public Access

Author manuscript

DNA Repair (Amst). Author manuscript; available in PMC 2022 July 19.

Published in final edited form as:

DNA Repair (Amst). 2018 April ; 64: 26–33. doi:10.1016/j.dnarep.2018.02.004.

XRCC1 phosphorylation affects aprataxin recruitment and DNA deadenylation activity

Julie K. Horton[1], **Donna F. Stefanick**[1], **Melike Çağlayan**[1], **Ming-Lang Zhao**[1], **Agnes K. Janoshazi**[2], **Rajendra Prasad**[1], **Natalie R. Gassman**[3], **Samuel H. Wilson**[1,*]

[1]Genome Integrity and Structural Biology Laboratory

[2]Fluorescence Microscopy and Imaging Center, Signal Transduction Laboratory, NIEHS, National Institutes of Health, Research Triangle Park, North Carolina 27709, USA

[3]Current address: Department of Oncologic Sciences, University of South Alabama Mitchell Cancer Institute, Mobile, Alabama 36604, USA

Abstract

Aprataxin (APTX) is a DNA-adenylate hydrolase that removes 5′-AMP blocking groups from abortive ligation repair intermediates. XRCC1, a multi-domain protein without catalytic activity, interacts with a number of known repair proteins including APTX, modulating and coordinating the various steps of DNA repair. CK2-phosphorylation of XRCC1 is thought to be crucial for its interaction with the FHA domain of APTX. In light of conflicting reports, the importance of XRCC1 phosphorylation and APTX function is not clear. In this study, a phosphorylation mutant of XRCC1 designed to eliminate APTX binding was stably expressed in *Xrcc1*$^{-/-}$ cells. Analysis of APTX-GFP accumulation at micro-irradiation damage confirmed that phosphorylated XRCC1 is required for APTX recruitment. APTX-mediated DNA deadenylation activity (*i.e.*, 5′-AMP removal) was measured in extracts of cells expressing wild-type XRCC1 or the XRCC1 phosphorylation mutant, and compared with activity in APTX-deficient and APTX-complemented human cells. APTX activity was lower in extracts from *Xrcc1*$^{-/-}$ and XRCC1 phosphorylation mutant cells compared to the robust activity in extract from wild-type XRCC1 expressing cells. Taken together, results verify that interaction with phosphorylated XRCC1 is a requirement for significant APTX recruitment to cellular DNA damage and enzymatic activity in cell extracts.

Keywords

XRCC1; APTX; DNA deadenylation

[*]**Corresponding Author:** Genome Integrity and Structural Biology Laboratory, NIEHS, National Institutes of Health, 111 T.W. Alexander Drive, P.O. Box 12233, Research Triangle Park, NC 27709, USA. Tel.; +1 919 541 4701; fax: +1 919 541 4724. wilson5@niehs.nih.gov (S.H. Wilson).

Conflict of Interest Statement: The authors declare that there is no conflict of interest.

1. Introduction

XRCC1 is a multi-domain protein without catalytic activity, but it interacts with a number of known repair proteins modulating and coordinating the various steps of base excision repair (BER) and single strand break repair (SSBR) [1]. Casein kinase 2 (CK2) is a constitutively active kinase that can phosphorylate numerous substrates associated with cellular stress responses. CK2 phosphorylates XRCC1 *in vivo* at as many as eleven consensus sites in the linker region between the BRCT I and BRCT II domains of the protein. Phosphorylated XRCC1 is a crucial scaffold protein interacting with aprataxin (APTX), as well as polynucleotide kinase 3′-phosphatase (PNKP) and aprataxin/PNK-like factor (APLF) [2-6], thus coordinating recruitment of these SSBR proteins. The fork-head associated (FHA) domain of APTX shares homology with the N-terminal FHA domain of PNKP [2] and is responsible for interaction with XRCC1. CK2-mediated phosphorylation of human XRCC1 serine/threonines at S518, T519, and T523 plays a crucial role in binding to APTX [5]. Mutation of these sites to alanine blocks phosphorylation by CK2 and decreases the binding affinity of APTX with XRCC1 [5]. Deficiency of XRCC1 leads to a reduction in APTX accumulation at sites of DNA damage and an impairment of SSBR [7]. APTX also binds XRCC4 in a phosphorylation-dependent manner [4, 8]. Phosphorylation of additional sites in the linker region between the BRCT I and BRCT II domains of human XRCC1 (S475, S485 and T488) is required to greatly stimulate the XRCC1-PNKP interaction [9]. Thus, the phosphorylation status of XRCC1 can strongly influence cellular repair.

Ataxia oculomotor apraxia-1 (AOA1) is a recessive human neurodegenerative disorder linked to more than 20 distinct mutations in the gene encoding APTX [4, 10]. Although reminiscent of ataxia-telangiectasia, primary AOA1 fibroblasts exhibit only mild hypersensitivity to ionizing radiation [4]. Mammalian DNA ligases interact with ATP forming a ligase-ATP complex; the activated ATP is then transferred to the 5′-phosphate of the nick in the form of AMP, eventually resulting in formation of a new phosphodiester bond and release of AMP. Abortive ligation intermediates with an adenylate (AMP) group at the 5′-phosphate end of the nicked DNA intermediate (5′-AMP) arise when DNA ligases attempt to ligate ‘dirty’ ends, including BER intermediates or 3′-modified or oxidized nucleotides produced during repair of damaged DNA [11, 12]. Where the 5′-deoxyribose phosphate (5′-dRP) intermediate of BER is 5′-adenylated to form the blocking 5′-AMP-dRP, APTX can remove the 5′-AMP leaving 5′-dRP and enabling resumption of BER [13]. In general, 5′-AMP intermediates are thought to be rare [14]. Nevertheless, cells express APTX to resolve abortive ligation products by removing the 5′-AMP blocking group in duplex DNA [4, 15–17]. APTX comprises three domains; the N-terminal FHA domain mentioned above binds to XRCC1 and PAR, whereas a central histidine triad (HIT) domain and a Cterminal zinc finger domain mediate catalytic activity and DNA interactions, respectively [14, 17].

PARP-1 recognizes and binds to DNA strand breaks stimulating vast synthesis of PAR polymers onto itself and other repair proteins [18]. The ADP-ribose of PAR polymers mediate recruitment of XRCC1 via binding at its BRCT 1 domain [19]. Mutations in this domain can prevent XRCC1 interaction with PAR, and inhibitors of PARP activity delays XRCC1 recruitment to sites of laser-induced DNA damage [20]. The FHA domain of APTX is reported to interact with the BRCT domain of PARP-1 [21], and also to PAR

but unlike XRCC1, the interaction is not with ADP-ribose group, but instead with the iso-ADPribose linkage between each PAR ADP-ribose [20]. FHA domain mutations of APTX can prevent the PAR interaction. It is suggested that the interaction with PAR mediates early recruitment of APTX to damaged sites. Since PAR is degraded rapidly following DNA damage, retention of APTX may result from its binding with other binding partners such as XRCC1. However, the relative contributions of the XRCC1 and PAR mediated interactions are unknown.

There are discrepancies in the literature regarding the role of the XRCC1/APTX interaction in BER/SSBR, and protection against DNA damaging agents. For example, one group proposed that interaction between XRCC1 and APTX is not required for survival after MMS [5], whereas another study documented MMS and hydrogen peroxide hypersensitivity in primary AOA1 fibroblasts and lymphoblastoid cell lines having no detectable APTX [4, 21].

Aiming to directly re-evaluate the consequence of elimination of the affinity of APTX for XRCC1, stably transfected mouse *Xrcc1*$^{-/-}$ cell lines were isolated expressing mouse XRCC1 mutated at S517A, T518A, T522A, and S524A (equivalent to human S518A, T519A, T523A and S525A) and designed to block phosphorylation by CK2 [5]. The MMS and CPT hypersensitivity of XRCC1-deficient mouse fibroblasts was first confirmed. Then, cells expressing the APTX phosphorylation mutant of XRCC1 or wild-type XRCC1 were evaluated for hypersensitivity to these two agents. In addition, recruitment of APTX-GFP to micro-irradiation damage was analyzed in these XRCC1-tranfected cells. Finally, APTX-mediated DNA deadenylation activity was measured in cell extracts of the XRCC1 variants, and compared with activity in patient AOA1 human fibroblasts and APTX-complemented cells. Taken together, results reveal that interaction with phosphorylated XRCC1 is a requirement for APTX recruitment and enzymatic activity, though not for cell survival following MMS- or camptothecin (CPT)-induced DNA damage.

2. Materials and methods

2.1. Isolation of phosphorylation-mutant and wild-type complemented XRCC1 cells

Xrcc1$^{+/+}$ and *Xrcc1*$^{-/-}$ p53-deficient mouse embryonic fibroblasts were obtained from Dr. Robert Tebbs [22]. These cells were maintained in low glucose DMEM (Invitrogen) supplemented with 10% FBS at 37 °C. A pEF-DEST51 vector containing mouse XRCC1 (pXR1) was created as described previously [23]. Mutations at S517A, T518A, T522A, and S524A (equivalent to human S518A, T519A, T523A and S525A) were introduced by site-directed mutagenesis of the pXR1 wild-type vector to produce pXPK. Additional mutations at mouse S474A, S484A, and T487A (equivalent to S475A, S485A and T488A in human) were introduced by site-directed mutagenesis of the pXPK vector to produce pXCKD. The mammalian cell expression vectors were sequence verified.

One day before transfection, 2×10^5 *Xrcc1*$^{-/-}$ cells were seeded in six-well dishes in 2 ml of growth medium without antibiotics so that cells would be 95% confluent at the time of transfection. Complexes were prepared as follows: 5 μg of DNA was diluted in 250 μl of DMEM without serum and mixed gently. Lipofectamine™ 2000 (Invitrogen) was mixed gently prior to use then diluted by adding 10 μl to 250 μl of DMEM and

incubated for 5 min at room temperature. The diluted DNA was combined with diluted Lipofectamine™ 2000. After transfection, cells were split into growth medium containing 10% FBS. Selection with blasticidin (10 mg/ml; Invitrogen) was initiated the following day and XPK single cell clones were isolated and screened for XRCC1 expression by western blotting. One clone (XPK4) was selected based on similar level of XRCC1 expression as *Xrcc1*$^{+/+}$ cells. A single XCKD clone (XCKD16), unable to interact with PNKP, has been described previously [24].

Complementing wild-type XRCC1 was expressed in *Xrcc1*$^{-/-}$ cells using lentivirus as described previously [25]. Lentiviral plasmid constructs for stable expression of mouse XRCC1 were created by PCR amplification of the XRCC1 gene from the pDONR221 vector [26] with primers that introduced NheI and NotI sites. The amplified XRCC1 was cloned into the pCDH-EF1-MCS-IRES-Puro (System Biosciences, Mountain View, CA) to produce pCDH532-XRCC1, which was sequenced verified. Lentivirus particles were produced by the NIEHS Viral Vector Core and packaged in HEK293T/17 cells (ATCC # CRL-11268) according to published Current Protocols in Neuroscience by P. Salmon and D. Trono. *Xrcc1*$^{-/-}$ cells were transduced with lentiviral particles at multiplicity of infection (MOI) of 20 per 50,000 cells, and stable cell lines were recovered after puromycin selection (6 μg/ml, Life Technologies). After characterization by western blot analysis (as described below), single cell clones were isolated from those demonstrating significant XRCC1 expression. One XRCC1 WT clone (XC5) was used in this study.

Human fibroblasts were a kind gift from Dr. Keith Caldecott. FD105 M20 (AOA1) is an uncorrected vector control hTERT immortalized AOA1 cell line derived from the primary cell line FD105. APTXFD105 M21 (APTX-comp) is an hTERT immortalized AOA1 patient fibroblast cell line corrected with full-length *APTX* cDNA under a constitutive expression promoter [16]. Western blotting of the AOA1 cell line confirmed the absence of APTX and the presence in the corrected cells [16]. Both cell lines were grown at 37 °C in Minimal Essential Medium (Invitrogen) supplemented with 5% FBS, puromycin (0.3 μg/ml) and G418 (300 μg/ml). Mycoplasma testing was performed routinely on all cell lines using a MycoAlert® Mycoplasma detection kit (Lonza, Rockland, ME).

2.2. Western blot analysis

Whole cell extracts were prepared as described previously [26, 27]. The protein concentration of the extracts was determined by the Bio-Rad assay. Extract samples (60 μg) were loaded onto 4–12% Bis-Tris NuPAGE gels (Invitrogen) and electrophoresed in NuPAGE MES running buffer at 4°C. Proteins were transferred to nitrocellulose filters in the cold for 4 h at 25 V and filters were blocked overnight at 4°C in 5% nonfat dry milk in Tris-buffered saline (TBS) with 0.1% Tween 20 (TBST). Transfer blots were first incubated for 2 h at room temperature or overnight at 4°C with mouse monoclonal anti-XRCC1 primary antibody (Thermo Fisher Scientific, 33–2-5). After washing, filters were incubated with goat anti-mouse IgG-horseradish peroxidase (HRP) conjugated secondary antibody (1:2,000–1:20,000 dilution, Bio-Rad) and visualized using Super Signal (Thermo Scientific). Blots were stripped in Restore Western Blot Stripping Buffer (Thermo Scientific), washed three times in TBST, and blocked in 5% nonfat dry milk/TBST overnight before probing

similarly with other primary antibodies. These included 18S anti-pol β [28], anti-ligase III-1F3 (GeneTex MS-LIG31-PX1) and mouse anti-human PARP-1 (BD Pharmingen 51–6639GR). Polyclonal anti-aprataxin antibody (Abcam ab66861), antiphospho (S518/T519/T523) XRCC1 (Bethyl Laboratories A300–059A) and anti-phospho (S485/T488) XRCC1 (Bethyl Laboratories A300–231A) were probed with goat anti-rabbit HRP conjugate. Probing with mouse monoclonal anti α-tubulin, clone DM 1A (Sigma T-9026) was used as a loading control.

2.3. Co-immunoprecipitation and immunoblotting

To examine XRCC1 interaction with APTX, equal amounts (200 μg protein) of cell lysate from XRCC1 WT and XPK4 cells were mixed with 0.5 μg of polyclonal IgG antibody specific to XRCC1 or 5 μl rabbit nonimmune serum. The mixture was incubated on ice for 2 h. Then, the immunocomplex was adsorbed onto a mixture (20 μl) of protein A-sepharose and protein G-sepharose beads by incubating the mixture overnight at 4 °C. The sepharose beads were washed 3 times with IP buffer (50 mM Tris-HCl, pH 7.5, 150 mM NaCl, 25 mM NaF, 0.1 mM sodium orthovanadate, 0.2 % Triton X-100, 0.3 % NP-40, and protease inhibitor cocktail). Finally, the beads were mixed in 25 μl SDS-PAGE sample buffer and heated for 5 min at 95 °C. Soluble proteins were separated by Nu-PAGE 4–12% Bis-Tris mini-gel electrophoresis and transferred onto a nitrocellulose membrane. The membrane was cut into two strips; strip A (representing proteins higher than 52 KDa molecular weight) and strip B (representing proteins lower than 52 KDa molecular weight). Both membrane strips were incubated in 5% nonfat dry milk in TBS-T. Strip A was probed with mouse monoclonal antibody to XRCC1 (1:1000 dilution, Ab 33–25, Abcam) and strip B was probed with monoclonal antibody to APTX (1:100 dilution, ab 192598, Abcam). Goat anti-mouse IgG conjugated to horseradish peroxidase (1:10,000 dilution) was used as secondary antibody, and the immobilized horseradish peroxidase activity was detected by enhanced chemiluminescence (ECL).

2.4. Cytotoxicity studies by growth inhibition assay

Cells were seeded (5–10,000 cells per well in six-well dishes) in medium without selection antibiotic. The next day, cells were treated for 1 h with a range of concentrations of MMS, or for 24 h with the Top1 inhibitor CPT. In other studies, cells were dosed with a combination of MMS plus 4-AN (5 μM for 24 h). After washing as appropriate, growth medium was added. Triplicate wells for each drug concentration were counted by a cell lysis procedure [26, 29] when untreated cells were 80% confluent, and results expressed as % control growth. Fold hypersensitivity was determined at IC_{90} concentrations, the dose required for 90% decrease in cell growth. For experiments with mouse fibroblasts, we find this growth inhibition assay to be more reliable and consistent than clongenic or short-term cytotoxicity assays. Results obtained are in agreement with alternate assay methods [26].

2.5. Immunofluorescence and micro-irradiation

For immunofluorescence (IF) studies, XRCC1 WT and XPK4 cells were seeded on 35 mm glass bottomed petri dishes containing an etched grid (MatTek, Ashland, MA) at 2×10^5 cells per dish and incubated for 24 h in growth medium supplemented with 10 μM BrdU. DNA single strand breaks (SSBs) and oxidized DNA base lesions, but not double strand

breaks (DSBs), were specifically introduced by micro-irradiation with a fiber-coupled 355 nm Coherent laser (maximum power 60 mW) via objective 40x C-Apochromat NA 1.2 Korr FCS M27 at an intensity equivalent to 0.165 uJ calculated as previously [30]. The irradiation strip size, region of interest (ROI), was manually drawn 0.45 μm across the nucleus for 200 μs (100 scanning iterations).

Previous studies had established that peak XRCC1 recruitment occurs 60 s after micro-irradiation in MEFs [30, 31]. Cells were fixed in 4% paraformaldehyde at times 30, 60, 120 and 180 s after irradiation and stained for IF. After fixation, cells were permeabilized with 0.25% Triton X-100 in PBS for 10 min, washed three times with PBS, then further permeabilized in 1% SDS for 5 min at 37 °C, washed six times with PBS, then blocked with 3% BSA in PBS for 60 min. Cells were then incubated with anti-XRCC1 antibody (1:50; Abcam ab1838) for 1 h. Cells were washed three times with PBS, then incubated with Alexa 488 conjugated anti-mouse secondary antibody (1:2,000; Life Technologies) for 1 h and cells were again washed three times with PBS. Fluorescence images were acquired with 512 × 512 pixels, bidirectional mode averaging of 2 lines, zoom 1.0 and pixel dwell time 3.5 μs with the same 40x water immersion objective on the Zeiss LSM780 microscope controlled by Zen 2012 SP2 software. Recruitment of XRCC1 at the site of DNA damage was analyzed using IMAGEJ and SigmaPlot (Systat Software Inc.) as described previously [30]. Each experiment was repeated, and images presented are representative.

For initial APTX recruitment studies, XRCC1 WT cells seeded in 35 mm glass bottomed petri dishes (MatTek, Ashland, MA) at 1×10^5 cells per dish were transiently transfected 24 h after plating using Lipofectamine™ 2000 and mouse C-terminal TurboGFP-APTX (MG 218020) purchased from Origene (Rockville, MD). Transfection medium was supplemented with 10 μM BrdU (Sigma-Aldrich). 24 h after transfection, medium was changed to fresh room temperature growth medium without BrdU. Only cells with similar low to moderate fluorescence intensities were analyzed.

DNA single strand breaks (SSBs) and oxidized DNA base lesions, but not double strand breaks (DSBs) [24], were specifically introduced by micro-irradiation with a fiber-coupled 355 nm Coherent laser (maximum power 60 mW) via objective 40x C-Apochromat NA 1.2 Korr FCS M27 at an intensity equivalent to 0.165 uJ calculated as previously [30]. The irradiation strip size, region of interest (ROI), was manually drawn 0.45 μm across the nucleus for 200 μs (100 scanning iterations) as described above. For GFP image acquisition in live-cell experiments, a 488 nm laser was used at 1% intensity to minimalize photo bleaching. Fluorescence emission of GFP was detected in the range of 491–580 nm using a pinhole of 40 μm. Fluorescent protein recruitment was recorded by a highly sensitive, new generation Gallium arsenide phosphide (GaAsP) *detector in photon counting mode, giving an order of magnitude more sensitivity than other photomultipliers in integral mode. This set up was necessary since fluorescent protein recruitment was not observed in cells with very high intensity expression. S*amples were imaged using a 40x C-Apochromat NA 1.2 Korr FCS M27 water immersion objective coupled to a Zeiss LSM780 confocal microscope (Carl Zeiss MicroImaging).

Three pre-bleach images were acquired to establish a base line prior to damage induction. Images were then acquired at room temperature every 3 s after the bleaching event for 200 s. Relative recruitment of fluorescent reporter was determined by measuring the signal intensity of GFP at the induced damage site in the ROI. Time-lapse recruitment curves were corrected by subtracting the post bleach signal intensity of the entire nucleus excluding the ROI. The experiment was repeated with fifteen cells and analyzed using SigmaPlot. After intensity normalization and setting the amplitude of the curve in the range 0–100%, data were plotted as mean relative recruitment ± SEM and fitted to a single exponential.

In other experiments APTX-GFP recruitment was compared in *Xrcc1*$^{-/-}$, XPK4 and XCDK16 cell lines. Data from at least fifteen cells were presented as normalized fluorescence intensity I_{max}/I_0, mean ± SEM over the 200 s time course. The effect of treatment with the PARPi, veliparib, on recruitment of APTX-GFP was also assessed. APTX-GFP transfected XRCC1 WT cells were either pre-treated or not (fifteen cells in each set) for 1 h with veliparib (10 μM), then irradiated in stripes. Recruitment of APTX-GFP was followed for 200 s still in the absence or presence of inhibitor. For PNKP recruitment studies, XRCC1 WT and XPK4 cells were transiently transfected 24 h after plating using Lipofectamine™ 2000 and human C-terminal TurboGFP-PNKP (RG207551) purchased from Origene (Rockville, MD). Data was acquired and analyzed as described above for APTX-GFP.

2.6. DNA deadenylation assay in cell extracts

Cell extracts were prepared from XRCC1 WT, *Xrcc1*$^{-/-}$ and XPK4 as described previously [26, 27]. Extracts were similarly prepared form vector control AOA1 immortalized human fibroblasts (AOA1) and AOA1 immortalized fibroblasts complemented with full length APTX cDNA (APTX-comp) [16]. Template DNA strand, upstream oligodeoxyribonucleotides and downstream primer with a 3'−6-carboxyfluorescein (FAM)-label were from Integrated DNA Technologies, Inc. Sequences of these oligonucleotides were reported previously [11]. The 5'-DNA adenylation kit was puchased from New England BioLabs (Ipswich, MA). The nicked double-stranded DNA substrate with adenosine monophosphate (AMP) at the 5'-end of the 3'-end FAM-labeled oligonucleotide was prepared as reported previously [11]. Recombinant human APTX enzyme used for control reactions was purchased from Fitzgerald (North Acton, MA). For the DNA deadenylation assays, the reaction mixture contained 50 mM Hepes, pH 7.5, 20 mM KCl, 0.5 mM EDTA, 2 mM DTT, and 100 nM DNA substrate (50 μl total volume). Positive control reactions were initiated by addition of 100 nM purified APTX with incubation for 15 min at 37°C. The assay was initiated by addition of cell extract (50 μg) and the reaction mixture was incubated at 37°C for the indicated time points before adding an equal volume of gel loading buffer (95% formamide, 20 mM EDTA, 0.02% bromphenol blue, and 0.02% xylene cyanol). The reaction products were separated in a 15% polyacrylamide gel containing 8 M urea in 89 mM Tris-HCl, 89 mM boric acid, and 2 mM EDTA, pH 8.8. The gels were scanned on a Typhoon PhosphorImager, and data were analyzed as previously [11, 13].

3. Results

3.1. Characterization of XRCC1 phosphorylation mutant-expressing cells

Stably transfected *Xrcc1*$^{-/-}$ cell lines were isolated expressing XRCC1 mutated at S517A, T518A, T522A, and S524A (equivalent to human S518A, T519A, T523A and S525A). One of the clones selected (XPK4) expressed a level of mutant protein similar to that of endogenous XRCC1 protein in *Xrcc1*$^{+/+}$ cells (Fig. 1A, compare lanes 1 and 3), whereas, as expected, *Xrcc1*$^{-/-}$ cells did not express XRCC1 protein (lane 2). XRCC1 WT complemented cells isolated for comparison, expressed approximately 2-fold higher level of XRCC1 than the endogenous protein in *Xrcc1*$^{+/+}$ cells (Fig. 1A, compare lanes 1 and 4). Western blotting with phospho-specific (human S518/T519/T523) XRCC1 antibody revealed XRCC1 phosphorylation in *Xrcc1*$^{+/+}$ and XRCC1 WT-complemented cells (lanes 1 and 4), but not in XPK4 cells (lane 3). As expected, probing with an alternate phospho-specific (human S485/T488) XRCC1 antibody at a site generally associated with PNKP binding [9, 24] was positive in all three XRCC1-expressing cell lines (Fig. 1A). The level of APTX was slightly lower in XPK4 cells than in *Xrcc1*$^{-/-}$ and XRCC1 WT cells (Fig. 1B). Immunoprecipitation with anti-XRCC1 antibody and immunoblotting for XRCC1 and APTX confirmed an interaction between wild-type XRCC1 and APTX proteins (Fig. 1C, lane 1). Importantly, this interaction was not present in XPK4 cells expressing the XRCC1 phosphorylation mutant (Fig, 1C, lane 3). APTX was not immunoprecipitated from either cell line with preimmune serum (Fig. 1C, lanes 2 and 4).

3.2. Effect of the XRCC1 phosphorylation mutant on MMS sensitivity and sensitization by PARP inhibition

Xrcc1$^{-/-}$ cells complemented with wild-type XRCC1 (XRCC1 WT) cells showed complete reversal of MMS and CPT hypersensitivity (Fig. S1). Significant complementation of both MMS and CPT sensitivity was also seen in XPK4 cells (Fig. S1). It had been reported that phosphorylation at these CK2 sites of XRCC1 expressed in CHO cells, and interaction with APTX were not required for survival after MMS [5]. Alternatively, there are APTX backup pathways that can complement deficiency in APTX activity in cells, such as short-patch BER involving pol β dRP lyase activity (for removal of entire 5′-adenylated-dRP) and long-patch BER involving FEN1 nucleotide excision activity (for removal of 5′-adenylated-dRP or 5′-AMP) [11, 13]. Other as yet undefined backup pathways may also be present.

Previous studies had indicated that maximal sensitization by PARP inhibition occurs following methylation damage and formation of a 5′-dRP-containing intermediate of DNA repair [32]. The PARPi, 4-AN, sensitized XPK4 cells to MMS-induced cytotoxicity (7-fold) (Fig. S1A), though to a lesser extent to that observed in *Xrcc1*$^{+/+}$ cells (22-fold) [33]. The MMS sensitivity of XPK4 in the presence of 4-AN was similar to the MMS sensitivity in *Xrcc1*$^{-/-}$ without PARPi (Fig. S1A).

The persisting low hypersensitivity of XPK4 cells to CPT (Fig. S1B), suggests that the APTX/XRCC1 interaction may play an unexpected minor role in repair of CPT-induced DNA damage in this cell background. Sensitivity to a clinical Top1 inhibitor, irinotecan, had been correlated with APTX expression level [34]. Repair of a CPT-trapped Top1 cleavage

complex does not produce a 5′-blocked intermediate and there was only low level 4-AN sensitization (approximately 2-fold) in XPK4 cells (data not shown) and as noted previously in *Xrcc1*$^{+/+}$ cells, no sensitization was observed in *Xrcc1*$^{-/-}$ cells [24].

3.3. Recruitment of APTX-GFP in XRCC1 mutant cells after micro-irradiation

The recruitment of APTX-GFP in XRCC1 WT, XPK4 and *Xrcc1*$^{-/-}$ cell lines was measured following laser micro-irradiation. Cells were transiently transfected with APTX-GFP and incubated with the sensitizer BrdU, then laser irradiated the following day. Cells with low to moderate intensities were chosen since *fluorescent protein recruitment could not be observed in cells with high intensity expression.* With the micro-irradiation protocol used, DNA SSBs and oxidatively generated base lesions, but not DSBs, are produced [24].

Typical images representing accumulation of APTX-GFP at damaged sites 2 min after irradiation are shown in Figure 2A for each cell type. Note, fluorescence intensity increased only in the ROI surrounding the induced damaged (Fig. 2A), and no recruitment was observed using a vector expressing only enhanced GFP [24]. The combined data from 15 cells of each type are represented graphically (Fig. 2B). In comparison to the rapid recruitment of APTX-GFP to sites of damage in XRCC1 WT cells, no recruitment was observed in cells expressing the XRCC1 phosphorylation mutant (XPK4) or in *Xrcc1*$^{-/-}$ MEFs where XRCC1 is absent (Fig. 2B). Additional IF experiments demonstrated equivalent recruitment of XRCC1 in XRCC1 WT and in XPK4 cells over the first 3 min following laser irradiation (Fig. S2). A representative image in both cell lines after 1 min is shown in Fig. S2A. Taken together, the data confirm that interaction with phosphorylated XRCC1 is a requirement for APTX recruitment to laser-induced DNA damage in MEFs.

Interestingly, the observed XPK4 cell hypersensitivity to CPT in this study (Fig. S1B), was similar to that shown previously in XCDK16 cells expressing XRCC1 with seven CK2 phosphorylation site mutants designed to block interaction with PNKP [24]. Interaction of phosphorylated XRCC1 with PNKP enhances PNKP activity and enhances repair of CPT-mediated DNA damage [2]. Perhaps the four phosphorylation site mutations in XPK4 are sufficient to prevent interaction with PNKP despite previous suggestions that additional mutations are required [5, 9]. To investigate this possibility, further recruitment experiments were conducted. First as anticipated, it was shown that APTX-GFP was not recruited in XPK16 cells containing three additional (seven total) CK2 phosphorylation mutation sites (Fig. S3A). In XPK4 cells (Fig. S3B), similar to results obtained previously in XCDK16 cells [24], there was only minimal recruitment of PNKP-GFP. These experiments confirm the hypothesis that the four point mutations in XPK4 cells are able to prevent PNKP/XRCC1 binding and PNKP recruitment and may result in the observed CPT hypersensitivity (Fig. S1B).

3.4. APTX-GFP recruitment in XRCC1 WT cells after micro-irradiation and effect of PARP inhibition

XRCC1 WT cells were transiently transfected with APTX-GFP, incubated with the sensitizer BrdU, then laser irradiated the following day as outlined above. The time-lapse recruitment curve (% normalized fluorescence intensity against time) represent data from 15

cells. Recruitment kinetics for APTX-GFP were fit to a single exponential, with a half-time of 15.6 ± 0.3 s (Fig. 3A). Over the 200 s time course monitored, the clinically utilized PARPi, veliparib, inhibited recruitment of APTX-GFP to micro-irradiation DNA damage in the XRCC1 WT cells (Fig. 3B).

3.5. APTX-mediated DNA deadenylation activity

Deadenylation assays were first conducted with extracts prepared from APTX-deficient AOA1 human fibroblasts (FD105 M21) and APTX-comp AOA1 cells (FD105 M20) [16]. The nicked double-stranded DNA substrate with a 5′-AMP group and the reaction product after 5′-AMP removal by APTX are illustrated in Fig. 4A. APTX-deficient AOA1 cells were completely devoid of DNA deadenylation activity suggesting that APTX is the only enzyme capable of 5′-AMP removal in this cell type under these reaction conditions. As expected, APTX complementation restored 5′-AMP removal activity (Fig. 4B, Fig. 6A). XRCC1 WT MEFs had high levels of DNA deadenylation activity (Fig. 5A, Fig. 6B), similar to the level in the APTX-comp cells. *Xrcc1*$^{-/-}$ and XPK4 had similar and low, but detectable, activity (Fig. 5A and B, Fig. 6B), confirming the requirement for phosphorylated XRCC1 to achieve a significant level of APTX-mediated 5′-AMP removal. Yet, the observable activity in these cells compared to APTX-deficient AOA1 cells suggests that APTX has minimal activity in cell extracts even in the absence of XRCC1 interaction. This result correlates well with the observation that APTX interaction with phosphorylated XRCC1 is a requirement for APTX recruitment to laser-induced DNA damage (Fig. 2B).

4. Discussion

Phosphorylated XRCC1 is a crucial scaffold protein that interacts with the FHA domain of APTX [3, 4]. It had been reported that phosphorylation at the APTX binding sites of XRCC1 expressed in CHO cells, and the interaction with APTX, were not required for survival after MMS [5]. The same authors suggested that an observed sensitivity to MMS in the absence of APTX was due to destabilization of XRCC1 [5]. Yet, in other reports, XRCC1 levels were not affected by APTX expression levels [7, 21]. Another study reported low level MMS and hydrogen peroxide hypersensitivity in primary AOA1 fibroblasts and lymphoblastoid cell lines having no detectable APTX [4, 21].

To address discrepancies in the literature on the role of the XRCC1 and APTX interaction in BER and SSBR, isogenic mouse cells were isolated that are XRCC1 wild-type or deficient in the XRCC1/APTX interaction, and then tested for protection against DNA damaging agents. Almost complete complementation of MMS sensitivity was seen in XPK4 cells (Fig. S1A), confirming an earlier observation that an XRCC1 and APTX interaction is not essential for protection against MMS. This result was not surprising, since in cells with functioning BER and SSBR, DNA ligation failure is a rare event.

In a panel of cancer cell lines, sensitivity to a clinical Top1 inhibitor, irinotecan, could be correlated with APTX expression level [34]. In the same publication, inactivation of APTX in DT40 cells sensitized cells to CPT leading to the suggestion that APTX levels could predict patient response [34]. Additionally, a Comet assay revealed accumulation of CPT-induced damage in AOA1 compared with wild-type cells, indicating involvement of APTX

in repair [35]. The low level and minor CPT hypersensitivities reported previously in APTX-deficient and mutant cells [4, 21] suggest that the requirement for DNA deadenylation by APTX at abortive ligation intermediates is a rare event in cells.

The remaining slight hypersensitivity to CPT found here in XPK4 cells (Fig. S1B) was comparable to that observed previously in XCKD16 cells containing seven CK2 phosphorylation mutation sites in XRCC1, and unable to recruit PNKP to laser-induced damage [24]. The bifunctional enzyme, PNKP, is known to be required for end cleaning during repair of CPT-induced DNA damage [36]. PNKP-GFP was similarly not recruited in XPK4 cells (Fig. S3B) and may explain the CPT hypersensitivity observed.

Recruitment kinetics for APTX-GFP could be fitted to a single exponential with a calculated half-time 15.6 ± 0.3 s (Fig. 3A). This half-time is slightly slower than reported previously for GFP-tagged XRCC1, PNKP, Tdp1 and pol β in the same XRCC1 WT cell line [24]. The PAR requirement for efficient recruitment of both XRCC1 and APTX to laser micro-irradiation damage (Fig. 3B) has been described previously [7, 20]. Following damage of HeLa cells by heavy ion irradiation, inhibition of PARP activity did not prevent recruitment of GFP-tagged APTX, but accumulation was delayed [16]. The heavy ion irradiation produced γ-H2AX positive breaks (possibly DSBs) in contrast to the SSBs and oxidized DNA base lesions delivered by micro-irradiation used here [16, 24]. Since PAR-modified PARP mediates recruitment of XRCC1 [19, 20] and APTX recruitment in wild-type cells is largely dependent on binding to XRCC1 (Fig. 2B); the APTX recruitment effect may result from inhibition of XRCC1 recruitment by PARP inhibition. However, the interaction of the FHA domain of APTX with PAR provides an alternate mechanism for the observed PARP inhibitor effect [20]. APTX-GFP recruitment data confirm that interaction with phosphorylated XRCC1 is a requirement for APTX recruitment to micro-irradiation damage (Fig. 2B). No APTX-GFP accumulation was observed in *Xrcc1*$^{-/-}$ cells where XRCC1 is absent or in phosphorylation mutant XPK4 cells where APTX cannot bind. However, there are conflicting results from previous studies where APTX recruitment to laser micro-irradiation damage was shown to be both XRCC1-independent [20] and XRCC1-dependent [7].

DNA deadenylation assays conducted on a 5′-AMP containing double-stranded oligonucleotide substrate with cell extracts prepared from AOA1 APTX-deficient human fibroblasts revealed no measurable products of 5′-AMP removal (Fig. 6A). Cells complemented with APTX had significant activity, indicating that APTX alone is responsible for deadenylation in these cells under these assay conditions (Fig. 6B). Similarly, in a previous publication utilizing nuclear extracts from AOA1 and wildtype lymphoblasts, no deadenylation was observed in the absence of APTX [16]. In a more recent publication using whole cell extracts from AOA1 lymphoblasts or *aptx* gene-deleted DT40 cells, low amounts of DNA deadenylation activity, able to partially complement APTX deficiency, were observed [13]. It is not known why these products could not be seen here under the same conditions, but in alternate cell lines. *Xrcc1*$^{-/-}$ and XPK4 cells had minimal activity compared with *Xrcc1*$^{+/+}$ cells (Fig. 6B) indicating that phosphorylated XRCC1 is required for significant deadenylation, but is not absolutely required for APTX activity. The low APTX activity in these MEF cells was greater than the activity observed in AOA1

APTX-deficient patient fibroblasts. Using a very different circular 5´-AMP DNA substrate, and nuclear extracts from XRCC1-proficient and -deficient CHO cell lines, XRCC1 did not enhance repair [37].

Taken together, our current results demonstrate that interaction with phosphorylated XRCC1 is a requirement for APTX recruitment to micro-irradiation damage sites and enzymatic activity in cell extracts. The absence of a consistent hypersensitivity (MMS and CPT) phenotype under conditions of APTX deficiency suggest that a requirement for APTX-mediated DNA deadenylation with these agents is a rare event in cultured cells, or there exists efficient back-up pathways for removal of 5´-adenylated repair intermediates.

Supplementary Material

Refer to Web version on PubMed Central for supplementary material.

Acknowledgements

The authors thank Lois Wyrick for help with figure preparation, the NIEHS Viral Vector Core Facility for assistance with the lentivirus expression vector, the NIEHS Protein Expression Core Facility for assistance with expression vector construction, C. Jeff Tucker and Erica Scappini in the NIEHS Fluorescence Microscopy and Imaging Center for their expert assistance with micro-irradiation studies and the NIEHS Flow Cytometry Center for help with flow cytometric analysis. We thank Dr. Keith Caldecott for the kind gift of human AOA1 cells.

Grant Support

This work was supported by the Intramural Research Program of the NIH, National Institute of Environmental Health Sciences (project number Z01 ES050158 and ES050159).

References

[1]. Caldecott KW, XRCC1 and DNA strand break repair, DNA Repair, (2003) 955–969. [PubMed: 12967653]

[2]. Whitehouse CJ, Taylor RM, Thistlethwaite A, Zhang H, Karimi-Busheri F, Lasko DD, Weinfeld M, Caldecott KW, XRCC1 stimulates human polynucleotide kinase activity at damaged DNA termini and accelerates DNA single-strand break repair, Cell, 104 (2001) 107–117. [PubMed: 11163244]

[3]. Date H, Igarashi S, Sano Y, Takahashi T, Takano H, Tsuji S, Nishizawa M, Onodera O, The FHA domain of aprataxin interacts with the C-terminal region of XRCC1, Biochem. Biophys. Res. Commun, 325 (2004) 1279–1285. [PubMed: 15555565]

[4]. Clements PM, Breslin C, Deeks ED, Byrd PJ, Ju L, Bieganowski P, Brenner C, Moreira MC, Taylor AM, Caldecott KW, The ataxia-oculomotor apraxia 1 gene product has a role distinct from ATM and interacts with the DNA strand break repair proteins XRCC1 and XRCC4, DNA Repair, 3 (2004) 1493–1502. [PubMed: 15380105]

[5]. Luo H, Chan DW, Yang T, Rodriguez M, Chen BP, Leng M, Mu JJ, Chen DQ, Songyang Z, Wang Y, Qin J, A new XRCC1-containing complex and its role in cellular survival of methyl methanesulfonate treatment, Mol. Cell Biol, 24 (2004) 8356–8365. [PubMed: 15367657]

[6]. Ali AA, Jukes RM, Pearl LH, Oliver AW, Specific recognition of a multiply phosphorylated motif in the DNA repair scaffold XRCC1 by the FHA domain of human PNK, Nucleic Acids Res., 37 (2009) 1701–1712. [PubMed: 19155274]

[7]. Hirano M, Yamamoto A, Mori T, Lan L, Iwamoto TA, Aoki M, Shimada K, Furiya Y, Kariya S, Asai H, Yasui A, Nishiwaki T, Imoto K, Kobayashi N, Kiriyama T, Nagata T, Konishi N, Itoyama Y, Ueno S, DNA single-strand break repair is impaired in aprataxin-related ataxia, Ann. Neurol, 61 (2007) 162–174. [PubMed: 17315206]

[8]. Cherry AL, Nott TJ, Kelly G, Rulten S, Caldecott KW, Smerdon SJ, Versatility in phospho-dependent molecular recognition of the XRCC1 and XRCC4 DNA-damage scaffolds by aprataxin-family FHA domains, DNA Repair, 35 (2015) 116–125. [PubMed: 26519825]

[9]. Loizou JI, El-Khamisy SF, Zlatanou A, Moore DJ, Chan DW, Qin J, Sarno S, Meggio F, Pinna LA, Caldecott KW, The protein kinase CK2 facilitates repair of chromosomal DNA single-strand breaks, Cell, 117 (2004) 17–28. [PubMed: 15066279]

[10]. Le Ber I, Moreira MC, Rivaud-Pechoux S, Chamayou C, Ochsner F, Kuntzer T, Tardieu M, Said G, Habert MO, Demarquay G, Tannier C, Beis JM, Brice A, Koenig M, Durr A, Cerebellar ataxia with oculomotor apraxia type 1: clinical and genetic studies, Brain, 126 (2003) 2761–2772. [PubMed: 14506070]

[11]. Çağlayan M, Batra VK, Sassa A, Prasad R, Wilson SH, Role of polymerase β in complementing aprataxin deficiency during abasic-site base excision repair, Nat. Struct. Mol. Biol, 21 (2014) 497–499. [PubMed: 24777061]

[12]. Çağlayan M, Horton JK, Dai DP, Stefanick DF, Wilson SH, Oxidized nucleotide insertion by pol beta confounds ligation during base excision repair, Nat. Commun, 8 (2017) 14045. [PubMed: 28067232]

[13]. Çağlayan M, Horton JK, Prasad R, Wilson SH, Complementation of aprataxin deficiency by base excision repair enzymes, Nucleic Acids Res., 43 (2015) 2271–2281. [PubMed: 25662216]

[14]. Jiang B, Glover JN, Weinfeld M, Neurological disorders associated with DNA strand-break processing enzymes, Mech. Ageing Dev, 161 (2017) 130–140. [PubMed: 27470939]

[15]. Ahel I, Rass U, El-Khamisy SF, Katyal S, Clements PM, McKinnon PJ, Caldecott KW, West SC, The neurodegenerative disease protein aprataxin resolves abortive DNA ligation intermediates, Nature, 443 (2006) 713–716. [PubMed: 16964241]

[16]. Harris JL, Jakob B, Taucher-Scholz G, Dianov GL, Becherel OJ, Lavin MF, Aprataxin, poly-ADP ribose polymerase 1 (PARP-1) and apurinic endonuclease 1 (APE1) function together to protect the genome against oxidative damage, Hum. Mol. Genet, 18 (2009) 4102–4117. [PubMed: 19643912]

[17]. Rass U, Ahel I, West SC, Actions of aprataxin in multiple DNA repair pathways, J. Biol. Chem., 282 (2007) 9469–9474. [PubMed: 17276982]

[18]. Amé JC, Spenlehauer C, de Murcia G, The PARP superfamily, Bioessays, 26 (2004) 882–893. [PubMed: 15273990]

[19]. El-Khamisy SF, Masutani M, Suzuki H, Caldecott KW, A requirement for PARP-1 for the assembly or stability of XRCC1 nuclear foci at sites of oxidative DNA damage, Nucleic Acids Res., 31 (2003) 5526–5533. [PubMed: 14500814]

[20]. Li M, Lu LY, Yang CY, Wang S, Yu X, The FHA and BRCT domains recognize ADPribosylation during DNA damage response, Genes Dev., 27 (2013) 1752–1768. [PubMed: 23964092]

[21]. Gueven N, Becherel OJ, Kijas AW, Chen P, Howe O, Rudolph JH, Gatti R, Date H, Onodera O, Taucher-Scholz G, Lavin MF, Aprataxin, a novel protein that protects against genotoxic stress, Hum. Mol. Genet, 13 (2004) 1081–1093. [PubMed: 15044383]

[22]. Tebbs RS, Flannery ML, Meneses JJ, Hartmann A, Tucker JD, Thompson LH, Cleaver JE, Pedersen RA, Requirement for the Xrcc1 DNA base excision repair gene during early mouse development, Dev. Biol, 208 (1999) 513–529. [PubMed: 10191063]

[23]. Horton JK, Stefanick DF, Gassman NR, Williams JG, Gabel SA, Cuneo MJ, Prasad R, Kedar PS, DeRose EF, Hou EW, London RE, Wilson SH, Preventing oxidation of cellular XRCC1 affects PARP-mediated DNA damage responses, DNA Repair, 12 (2013) 774–785. [PubMed: 23871146]

[24]. Horton JK, Stefanick DF, Zhao M-L, Janoshazi AK, Gassman NR, Seddon HJ, Wilson SH, XRCC1-mediated repair of strand breaks independent of PNKP binding, DNA Repair, 60 (2017) 52–63. [PubMed: 29100039]

[25]. Horton JK, Seddon HJ, Zhao ML, Gassman NR, Janoshazi AK, Stefanick DF, Wilson SH, Role of the oxidized form of XRCC1 in protection against extreme oxidative stress, Free Radic. Biol. Med, 107 (2017) 292–300. [PubMed: 28179111]

[26]. Horton JK, Stefanick DF, Prasad R, Gassman NR, Kedar PS, Wilson SH, Base excision repair defects invoke hypersensitivity to PARP inhibition, Mol. Cancer Res, 12 (2014) 1128–1139. [PubMed: 24770870]

[27]. Biade S, Sobol RW, Wilson SH, Matsumoto Y, Impairment of proliferating cell nuclear antigen-dependent apurinic/apyrimidinic site repair on linear DNA, J. Biol. Chem, 273 (1998) 898–902. [PubMed: 9422747]

[28]. Singhal RK, Prasad R, Wilson SH, DNA polymerase β conducts the gap-filling step in uracil-initiated base excision repair in a bovine testes nuclear extract, J. Biol. Chem, 270 (1995) 949–957. [PubMed: 7822335]

[29]. Butler WB, Preparing nuclei from cells in monolayer cultures suitable for counting and for following synchronized cells through the cell cycle, Anal. Biochem, 141 (1984) 70–73. [PubMed: 6496937]

[30]. Gassman NR, Stefanick DF, Kedar PS, Horton JK, Wilson SH, Hyperactivation of PARP triggers nonhomologous end-joining in repair-deficient mouse fibroblasts, PLoS ONE, 7 (2012) e49301.

[31]. Masaoka A, Gassman NR, Kedar PS, Prasad R, Hou EW, Horton JK, Bustin M, Wilson SH, HMGN1 protein regulates poly(ADP-ribose) polymerase-1 (PARP-1) self-PARylation in mouse fibroblasts, J. Biol. Chem, 287 (2012) 27648–27658. [PubMed: 22736760]

[32]. Horton JK, Wilson SH, Predicting enhanced cell killing through PARP inhibition, Mol. Cancer Res, 11 (2013) 13–18. [PubMed: 23193155]

[33]. Horton JK, Watson M, Stefanick DF, Shaughnessy DT, Taylor JA, Wilson SH, XRCC1 and DNA polymerase β in cellular protection against cytotoxic DNA single-strand breaks, Cell Res., 18 (2008) 48–63. [PubMed: 18166976]

[34]. Dopeso H, Mateo-Lozano S, Elez E, Landolfi S, Ramos Pascual FJ, Hernandez-Losa J, Mazzolini R, Rodrigues P, Bazzocco S, Carreras MJ, Espin E, Armengol M, Wilson AJ, Mariadason JM, Ramon YCS, Tabernero J, Schwartz S Jr., Arango D, Aprataxin tumor levels predict response of colorectal cancer patients to irinotecan-based treatment, Clin. Cancer Res, 16 (2010) 2375–2382. [PubMed: 20371676]

[35]. Mosesso P, Piane M, Palitti F, Pepe G, Penna S, Chessa L, The novel human gene aprataxin is directly involved in DNA single-strand-break repair, Cell. Mol. Life Sc.i, 62 (2005) 485–491.

[36]. Weinfeld M, Mani RS, Abdou I, Aceytuno RD, Glover JN, Tidying up loose ends: the role of polynucleotide kinase/phosphatase in DNA strand break repair, Trends Biochem. Sci, 36 (2011) 262–271. [PubMed: 21353781]

[37]. Akbari M, Sykora P, Bohr VA, Slow mitochondrial repair of 5'-AMP renders mtDNA susceptible to damage in APTX deficient cells, Sci. Rep, 5 (2015) 12876. [PubMed: 26256098]

Highlights

- Phosphorylation of XRCC1 critical for its interaction with the FHA domain of APTX
- Expression of XRCC1 phosphorylation mutant designed to eliminate APTX binding
- Phosphorylated XRCC1 required for APTX-GFP recruitment at micro-irradiation damage
- Phosphorylation of XRCC1 greatly enhanced APTX-mediated DNA deadenylation activity

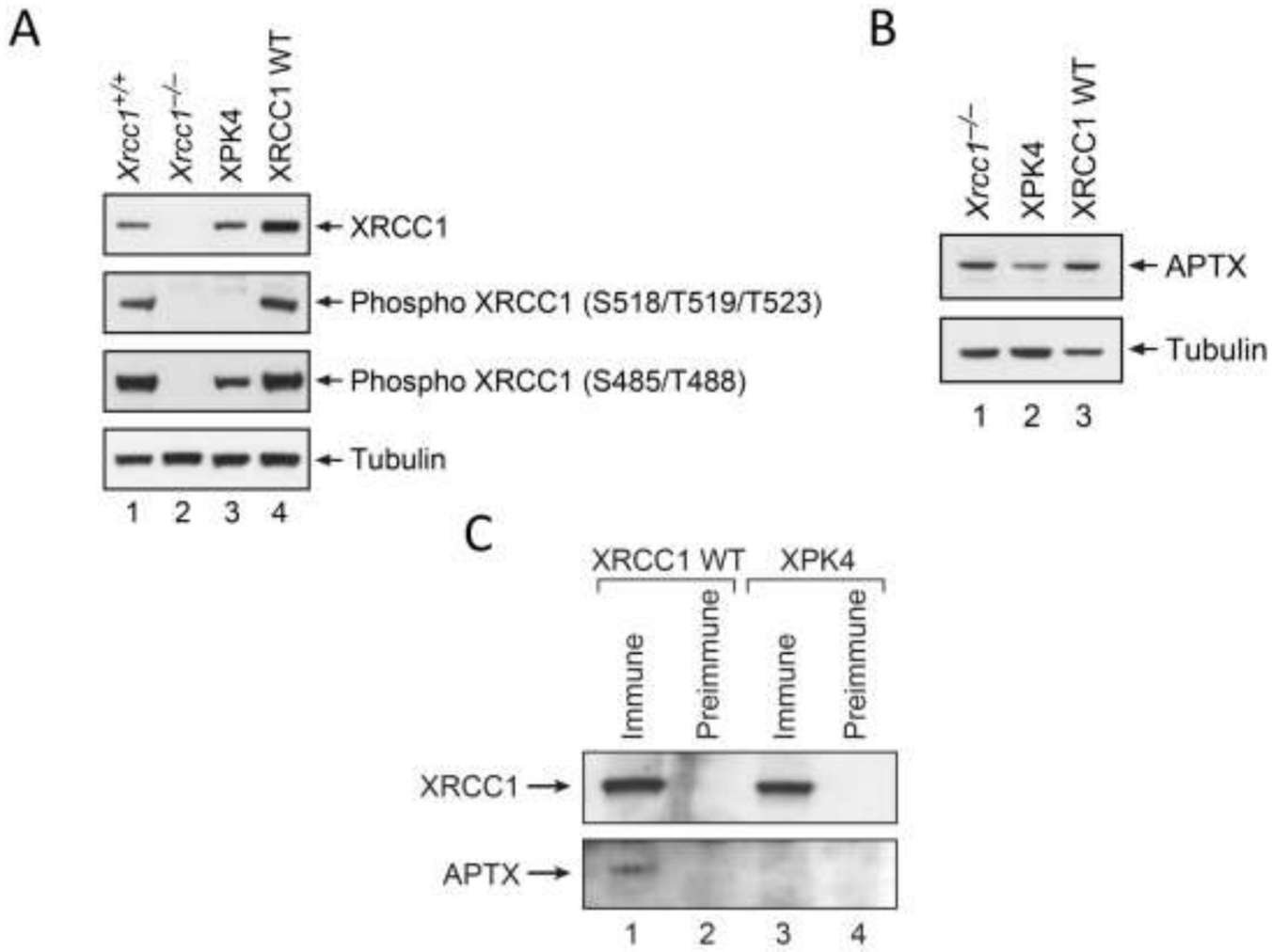

Fig. 1 –.

Characterization of XPK4 cells expressing the XRCC1 phosphorylation mutant. (A) Western blotting analysis of XRCC1 and phospho XRCC1 in XPK4 MEFs compared with *Xrcc1*$^{+/+}$, *Xrcc1*$^{-/-}$ and XRCC1 WT cells. (B) Expression of APTX in the same cell lines. Tubulin was used as a loading control. (C) Immunoprecipitation with XRCC1 antibody or preimmune serum from XRCC1 WT and XPK4 cell extracts, and immunoblot detection of XRCC1 and APTX. Full methods are given in Materials and Methods.

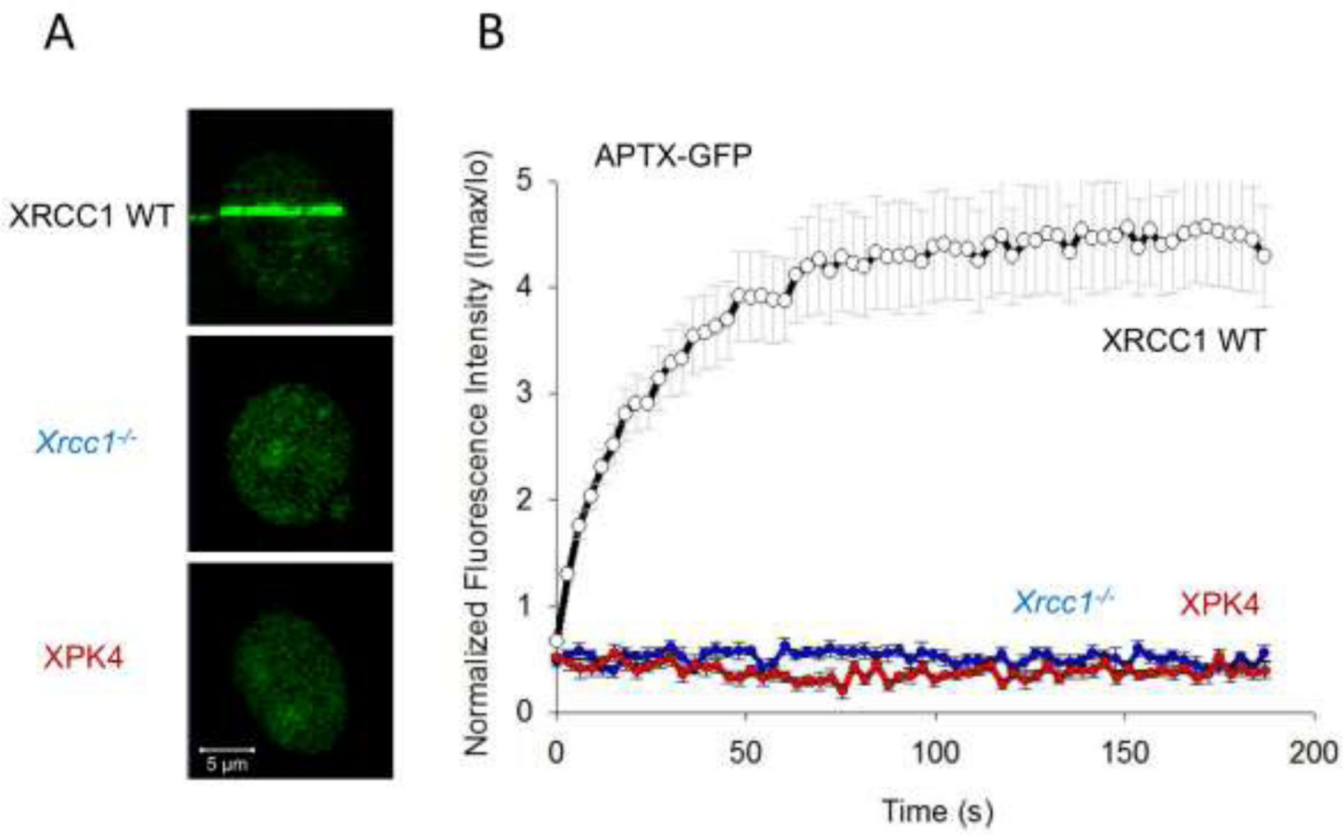

Fig. 2 –.

Recruitment of transiently expressed APTX-GFP to micro-irradiation damage sites. (A) Typical accumulation of APTX-GFP at damaged sites 2 min after irradiation in XRCC1 WT, *Xrcc1*$^{-/-}$ and XPK4 cells. (B) Graphical representation of 200 s time course of recruitment. Fluorescence data were normalized using the intensity at the beginning of recruitment (Io) and maximal intensity values (Imax), 15 cells of each type were analyzed, error bars represent SEM. Transfection and recruitment methods, are provided in Materials and Methods.

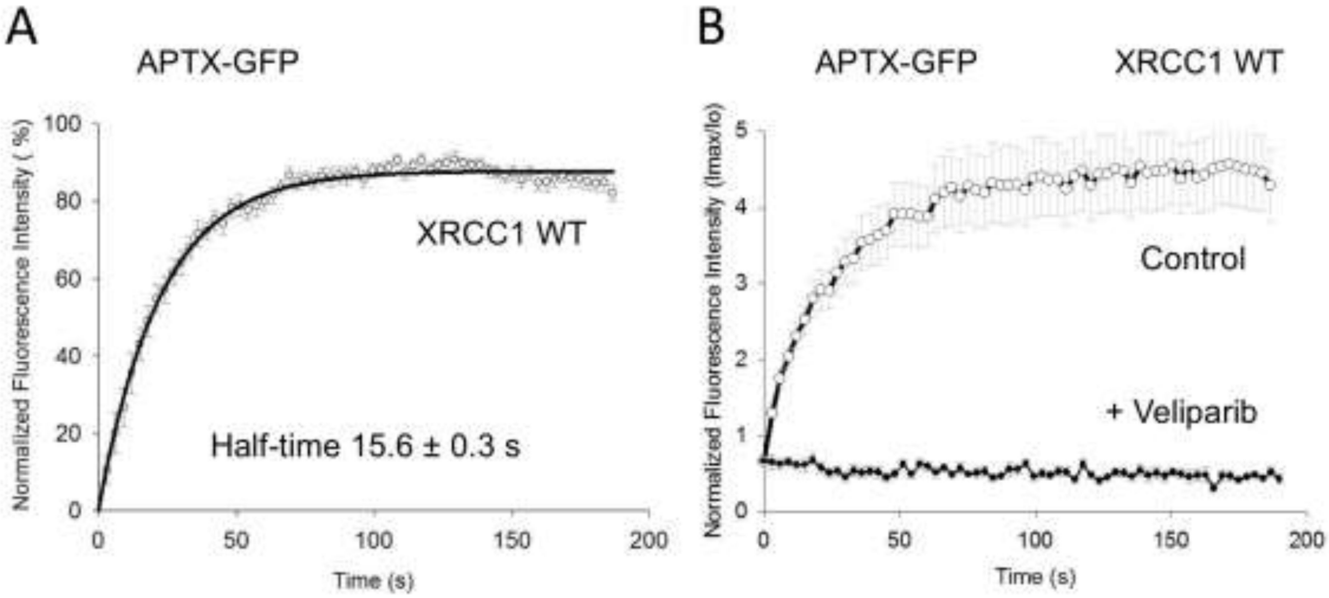

Fig. 3 –.

Time course of recruitment of transiently expressed APTX-GFP. (A) XRCC1 WT cells were subjected to micro-irradiation damage and recruitment of APTX-GFP was followed for 200 s (n = 15). Methods for transfection and recruitment, and data analysis are provided in Materials and Methods. Fluorescence data were normalized and recruitment kinetics were fitted to a single exponential. Error bars represent SEM. (B) Effect of PARP inhibition on recruitment of APTX-GFP. Transfected XRCC1 WT cells were pre-treated for 1 h with PARPi (veliparib), then irradiated in stripes. Recruitment was followed for 200 s in the absence or presence of veliparib (10 μM). 15 cells of each transfection and treatment condition were analyzed, error bars represent SEM. Experiments and data analysis are described in Materials and Methods.

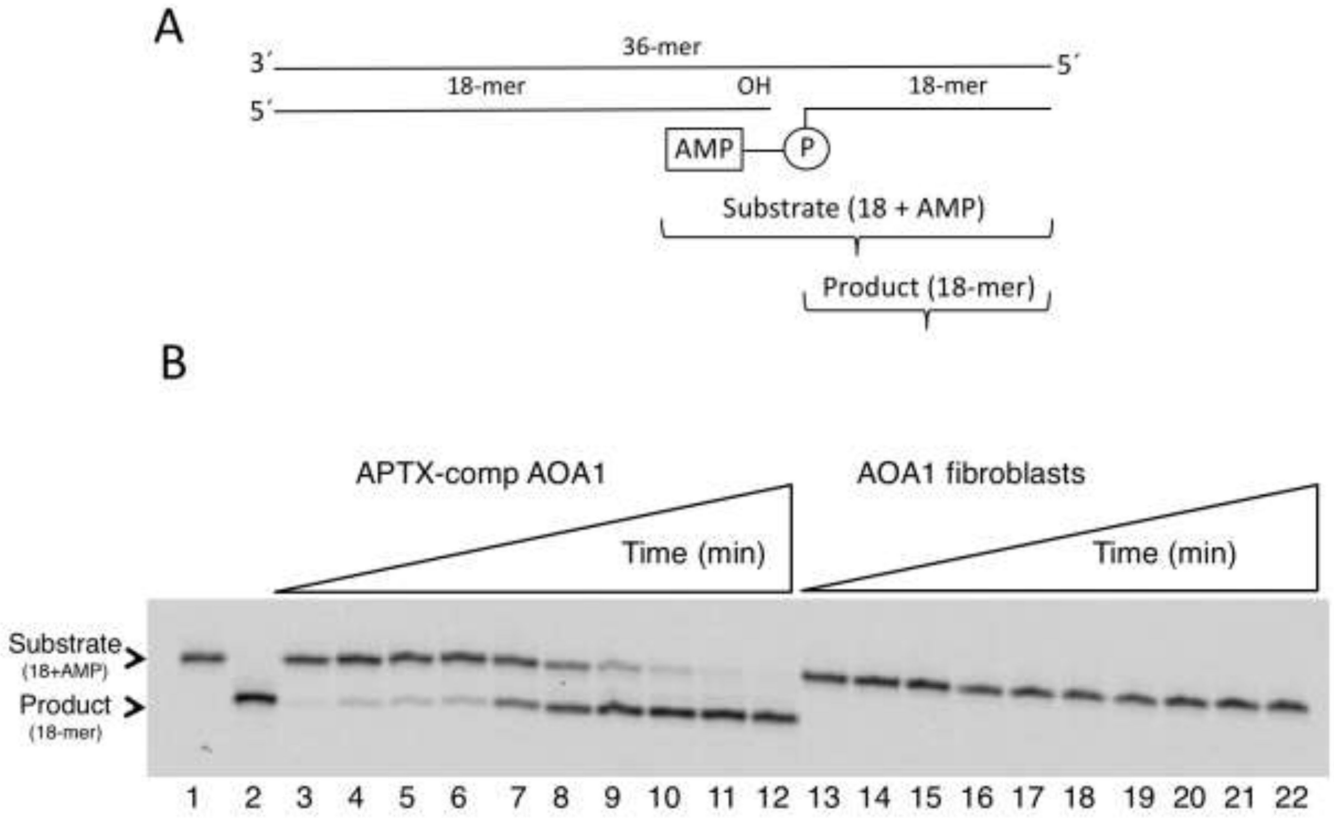

Fig. 4 –.

Comparison of APTX-mediated DNA deadenylation activity in human cell extracts. (A) Schematic representation of the nicked DNA substrate with 5′-AMP group (18+AMP) and expected reaction product (18-mer) after 5′-AMP removal. (B) Representative gel image of time course (0 – 10 min) showing 5′-AMP removal in human APTX-comp AOA1 fibroblasts (lanes 3–12) and vector control AOA1 cells (lanes 13–22). Lane 1 is a minus enzyme control, and lane 2 is a reference reaction using purified APTX. The quantification of the data is presented in Fig. 6A.

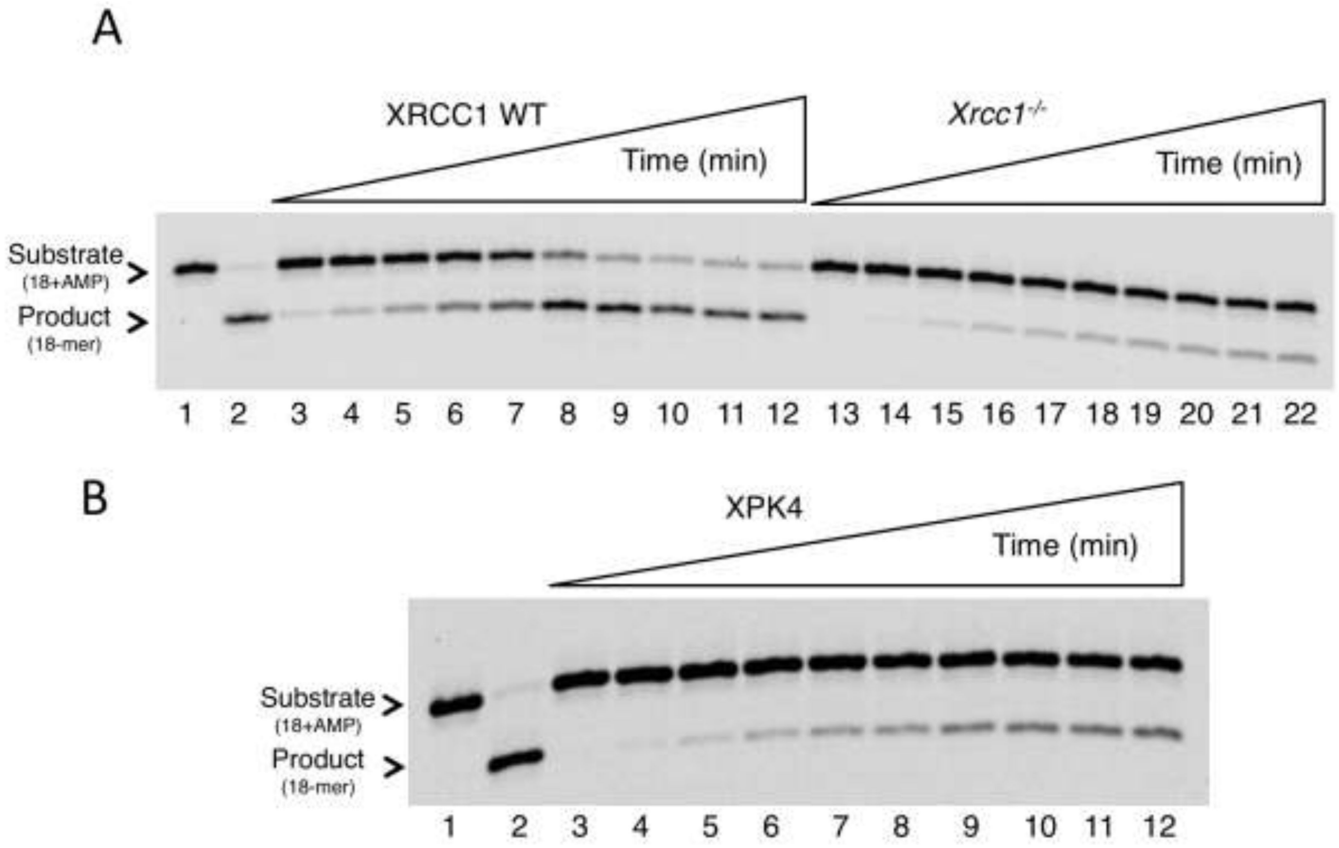

Fig. 5 –.

Comparison of DNA deadenylation activity in mouse XRCC1 cell extracts. (A) Representative gel image of time course (0 – 10 min) showing 5′-AMP removal in XRCC1 WT (lanes 3–12) and *Xrcc1*$^{-/-}$ mouse fibroblasts (lanes 13–22). (B) Similar time course in XPK4 cells (lanes 3–12). The quantification of the data is presented in Fig. 6B. Lane 1 is a minus enzyme control, and lane 2 is a reference reaction using purified APTX. Substrate and expected reaction product are as illustrated in Fig. 4A.

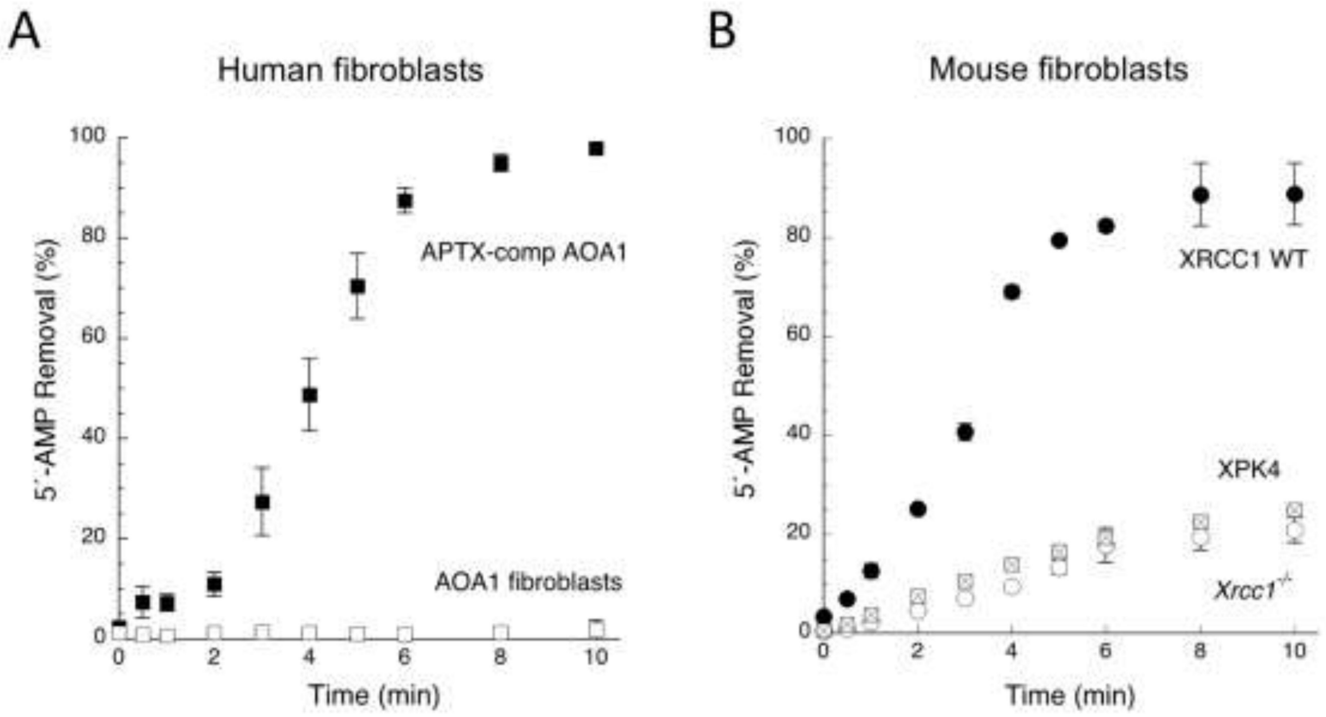

Fig. 6 –.

Comparison of APTX-mediated DNA deadenylation activity in cell extracts. (A) Time course of 5´-AMP removal in APTX-deficient human AOA1 fibroblasts and cells complemented with APTX. (B) Time course of activity in XRCC1 WT, *Xrcc1*$^{-/-}$ and XPK4 cells. DNA deadenylation assays are described in Materials and Methods. Plotted are mean ± SEM values obtained from at least 3 independent experiments.